Journal of The Electrochemical Society, **161** (14) A2204-A2209 (2014)
0013-4651/2014/161(14)/A2204/6/$31.00 © The Electrochemical Society

A Rotating Ring Disk Electrode Study of the Oxygen Reduction Reaction in Lithium Containing Dimethyl Sulfoxide Electrolyte: Role of Superoxide

Walter Torres, Nataliia Mozhzhukhina, Alvaro Y. Tesio, and Ernesto J. Calvo[z]

INQUIMAE, Facultad de Ciencias Exactas y Naturales, Ciudad Universitaria, AR-1428 Buenos Aires, Argentina

We have employed the rotating ring disk electrode (RRDE) technique to study the oxygen reduction reaction (ORR) on gold and glassy carbon cathodes in dimethyl sulfoxide (DMSO) electrolytes containing lithium salts. At the gold ring electrode at 3.0 V vs. Li/Li^+ (0.1 M $LiPF_6$) soluble superoxide radical anion undergoes oxidation to O_2 under convective-diffusion conditions. For both glassy carbon and gold cathodes, typical oxygen reduction current-potential curves are sensitive to rotation speed and undergo a maximum and further electrode passivation by formation of Li_2O_2 while the Au ring electrode currents follow the same peak shape with detection of soluble superoxide at the ring downstream in the electrolyte solution. Unlike the behavior in acetonitrile-lithium solutions, LiO_2 is more stable in DMSO and can diffuse out in solution and be detected at the ring electrode. While in cyclic voltammetry both time and potential effects are convoluted, we have carried out RRDE chrono-amperometry experiments at the disk electrode with detection of superoxide at the Au ring so that thus potential and time effects were clearly separated. The superoxide oxidation ring currents exhibit a maximum at 2.2 V due to the interplay of O_2^- formation by one-electron O_2 reduction, Li_2O_2 disproportionation and two-electron O_2 reduction.
 [DOI: 10.1149/2.0801414jes]

Manuscript submitted August 12, 2014; revised manuscript received October 10, 2014. Published October 25, 2014.

The rechargeable lithium-air battery exhibits a very large theoretical energy density that can compete with fossil fuels for electric vehicle applications with extended millage range.[1–4] The non aqueous Li-air battery introduced in 1996 by Abraham,[5] consists of a lithium metal anode that dissolves in non aqueous electrolyte and the resulting Li^+ ions react with oxygen reduction products to form insoluble lithium peroxide Li_2O_2 at a porous carbon cathode during discharge. Bruce et. al.[6] earlier showed that the electrochemical reaction of Li^+ with O_2 to yield insoluble Li_2O_2 in non aqueous electrolyte is reversible sustaining at that time more than ten charge/ discharge cycles.

The electrode kinetics of the oxygen reduction reaction (ORR) in lithium air battery cathodes strongly depends on the solvent,[7–9] electrolyte cation[10] and electrode material. On carbon and gold electrodes the first electroreduction product, superoxide is stable in non aqueous solutions containing tetra alkyl ammonium cations. In the presence of lithium ions superoxide is unstable in most aprotic solvents and yields insoluble lithium peroxide on the electrode surface.

Among non aqueous solvents, DMSO with a very large dipolar moment ($\mu = 4{,}06$ D)[11] and the appropriate geometry to coordinate Li^+ ions has been recently proposed for rechargeable Li-O_2 batteries.[12] Peng et. al. have claimed that the Li-air battery can be recharged with 95% capacity retention in 100 cycles using dimethyl sulfoxide (DMSO) electrolyte and porous gold electrode.[13] The stability of DMSO with respect to the nucleophillic attack by soluble superoxide ion produced by the oxygen reduction reaction (ORR) in the aprotic solvent has been demonstrated recently by in situ infrared subtractively normalized interfacial Fourier transform infrared spectroscopy (SNIFTIRS) experiments with large volume to surface ratio.[14] These studies also showed that DMSO is electrochemically oxidized to dimethyl sulfone on gold above 4.2 V so that it is imperative to reduce the recharge over potential. More recently the group of Bruce reported the advantage of recharging the Li-O_2 battery at 1 $mA.cm^{-2}$ and low over potential (c.a. 3.5 V) by incorporating a soluble TTF redox mediator with complete reversibility after 100 cycles.[15] Laoire et. al. reported the influence of non-aqueous solvents on the electrochemistry of oxygen in rechargeable lithium-air batteries[7] and compared the ORR in acetonitrile and DMSO electrolytes containing lithium ions. Trahan et. al.[9] reported studies of Li-Air cells in dimethyl sulfoxide-based electrolyte using the rotating disk (RDE) and rotating ring disk electrode (RRDE) and demonstrated that unlike acetonitrile in DMSO electrolyte soluble superoxide radical anion, O_2^-, can be collected at the ring electrode of the RRDE. In a recent communication we reported that soluble superoxide radical anion can be detected at a ring electrode of a RRDE system in lithium solutions of acetonitrile containing 0.1 M DMSO, unlike in pure acetonitrile lithium electrolytes which show no evidence of producing soluble O_2^-.[16] Therefore the stronger solvation of Li^+ in DMSO with respect to CH_3CN stabilizes solvated Li-O_2^- ion pairs as shown by molecular dynamic simulations.[17]

There are several experimental reports with evidence of DMSO oxidation by reactive oxygen species and lithium oxides during the reduction of oxygen on carbon and gold electrodes.[10,18–21] McCloskey et. al.[22] have shown that the balance of oxygen consumed in the ORR and that evolved in the OER during charging is always less than 0.9 due to the heterogeneous chemical reaction of the solid peroxide with the electrolyte or the carbon cathode.

In the present study we have used RRDE cyclic voltammetry and chronoamperometry to investigate the mechanisms of oxygen reduction in $LiPF_6$/DMSO electrolyte on glassy carbon and gold electrodes. The Au ring polarized at a potential where O_2^- is oxidized under convective-diffusion conditions collects soluble superoxide produced at the disk electrode in the course of the ORR. Chronoamperometry, used for the first time in this study, allows the distinction of time and potential effects on the electrode kinetics.

Experimental

Chemicals and solutions.— Anhydrous dimethyl sulfoxide, ≥99.9% **(SIGMA-ALDRICH),** tetra butyl ammonium hexafluoride phosphate for electrochemical analysis, ≥99.0% **(FLUKA),** lithium hexafluoride phosphate battery grade, ≥99.99% trace metals basis (ALDRICH), were stored in the argon-filled MBRAUN glove box with the oxygen content ≤ 0.1 ppm and water content below 2 ppm. Dimethyl sulfoxide was dried for several days over molecular sieves, 3 Å (SIGMA-ALDRICH); tetra butyl ammonium hexafluoride phosphate, lithium hexafluoride-phosphate, potassium dioxide and lithium peroxide were used as received. All solutions were prepared inside of the glove box and the water content was measured using the Karl Fisher 831 KF Coulometer (Metrohm). Solutions were found to contain around 50 ppm of water. It should be stressed that not only the initial concentration of water traces in DMSO solutions was measured, but periodically during the experiment the amount of water was checked by Karl Fisher technique. In long term experiments of several hours we observed that in spite of all precautions and low humidity in the acrylic box, the amount of water measured in lithium containing DMSO electrolyte increased. Therefore, short term experiments with freshly prepared solutions and short exposure to dry air were preferred.

[z]E-mail: calvo@qi.fcen.uba.ar

Electrochemical experiments.— Electrochemical experiments were performed in an air-tight acrylic box filled with Ar and dried with phosphorous pentoxide keeping a positive pressure by a stream of dry oxygen (see SI). The motor controller, motor and disk and ring mercury contacts in the bearing block are located outside the air-tight acrylic box and sealed with a rubber ring with a permanent flow of dry oxygen in the box. The electrochemical cell and RRDE cylinder immersed in the aprotic electrolyte were kept inside the box. This box contained the four-electrode glass cell and the electrolyte was fed from bottles filled in the glove box by a system needles and Teflon tubes without contact with the atmosphere. Large area platinum gauze was used as counter electrode in a compartment separated from the main compartment by a fritted glass.

A non-aqueous Ag/Ag^+ reference electrode was prepared by placing a silver wire in a fritted glass compartment filled with a 0.01 $AgNO_3$ solution in acetonitrile (0.1 M of tetra butyl ammonium hexafluoride phosphate was added to the solution to increase conductivity). The reference electrode was calibrated with respect to Li/Li^+ couple, that is commonly used as reference in Li-air battery studies. Inside the argon glove box, a Ag/Ag^+ electrode and a 3.2 mm diameter Li wire (99.9% trace metals basis **ALDRICH)** were placed in a beaker filled with 0.1 $LiPF_6$ in DMSO and the cell potential was measured with a high impedance voltmeter obtaining 3.7 V. It is worth mentioning that the potential measured between the same electrode and Li metal in a 0.1 M $LiPF_6$ solution in acetonitrile was 3.23 V that is 0.47 V lower than in DMSO solution. This difference is explained by an important Li^+ solvation energy difference between DMSO and acetonitrile. Further potential calibration was done with ferrocene in the DMSO solution.

Several rotating ring disk electrode systems have been employed as shown in Table I. In all cases both disk and ring were embedded in Araldite epoxy resin cylindrical body (Ciba-Geigy).

The geometrical area of the disk electrode was in all cases 0.196 cm^2. The geometric collection efficiency was calculated using the Albery-Hitchman theory[23] and experimentally verified with the $Fe(CN)_6^{4/3-}$ redox couple in a galvanostatic experiment. Soluble superoxide was detected at the ring electrode by convective-diffusion oxidation current at E_R = 3.0 V vs Li/Li^+ in DMSO. In previous experiments we have employed a platinum ring[16] but a residual ring current was detected due to the electrochemical oxidation of DMSO[14] so that a gold ring was employed in the present study (GC/Au and Au/Au RRDE).

Results and Discussion

The electrochemical behavior of the ORR in Li^+ ion containing DMSO electrolyte shows cathodic currents that reach a peak which increases with rotating frequency but are below the convective-diffusion Levich current:[7,24]

$$I_L = 1.554nFAD_{O_2}^{2/3}\nu^{-1/6}C_{O_2}W^{1/2} \quad [1]$$

where F is the Faraday constant, n the number of electrons per O_2 molecule, A the electrode geometric area, D_{O2} the O_2 diffusion coefficient in DMSO, c.a. 1.67×10^{-5} cm^2s^{-1},$C_{O2} = 2.1\times10^{-3}$ M,[7] the kinematic viscosity, ν = 0.0019 cm^2s^{-1},[7] A = 0.2 cm^2 , and W ($f = 2\pi\omega$) the rotation frequency in Hz. For n = 1 the expected values at 2 Hz (120 rpm) and 25 Hz (1500 rpm) are respectively 170 and 600 μA respectively.

Figures 1 and 2 depict the cyclic voltammetry of a Au and GC electrodes respectively in oxygen saturated 0.1 M $LiPF_6$ solution at a sweep rate of 100 $mV.s^{-1}$ when the electrode potential was linearly scanned between 4.7 to 1.9 V at 100 $mV.s^{-1}$. In the reducing sweep current maxima are apparent with further passivation of the electrode.

Table I. Geometric dimensions of RRDE used and the respective calculated and experimental collection efficiencies.

Electrode	r1	r2	r3	No Calc.	No Exp.
GC/Au	0.25	0.26	0.31	0.32	0.32
Au/Au	0.25	0.26	0.30	0.29	0.28

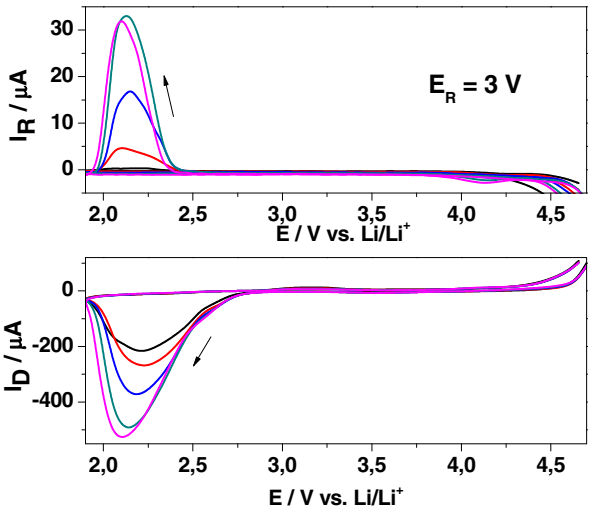

Figure 1. O_2 reduction polarization curve on a Au disk electrode in O_2 (1 atm) saturated 0.1 M $LiPF_6$ in anhydrous DMSO at W = 2, 4, 9, 16 and 25 Hz (ω = 60.W, in rpm) and scan rate of 0.1 V s^{-1} (lower panel) and O_2^- oxidation Au ring currents at E_R = 3 V (upper panel). A_D = 0.2 cm^2.

The corresponding convective-diffusion soluble superoxide oxidation current at the Au ring electrode simultaneous to the ORR are shown in the upper panels of Figures 1 and 2 for Au and GC disks electrodes respectively. Both disk and ring currents increase with rotation frequency and ring current maxima at 2.1 and 2.3 V respectively for Au and GC disk electrodes are observed (upper panel in Figs. 1 and 2). These results are consistent with previous reports.[9,16]

It should be noted from Figures 1 and 2 that glassy carbon is less reactive than gold with lower peak current at the same rotation speed. However, lower polarization and higher yield of superoxide are observed for glassy carbon. This may be due to the interaction of insoluble Li_2O_2 with the respective surfaces. On HOPG for instance the lithium peroxide deposits first at terrace edges and the surface is never totally passivated unlike gold.[25] The type of electrode surface may play an important role on the formation of solid insoluble lithium peroxide and surface passivation by the insulating

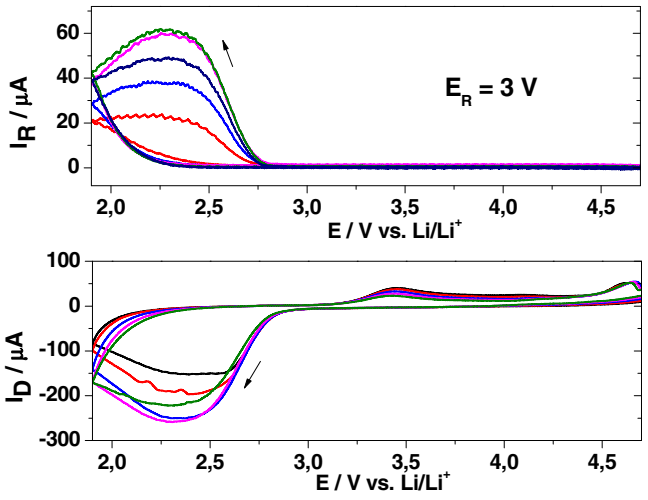

Figure 2. Cyclic voltammetry of a GC/Au RRDE at 0.1 $V.s^{-1}$ in O_2 (1 atm) saturated 0.1 M $LiPF_6$ in DMSO under convective-diffusion regime at W = 2,4, 9,16 and 25 Hz. (ω = 60.W, in rpm) (lower panel) and O_2^- oxidation Au ring currents at E_R = 3 V (upper panel). A_D = 0.2 cm^2.

peroxide. Possibly soluble lithium superoxide forms at the carbon surface which is not covered by lithium peroxide and thus a larger yield of soluble superoxide is collected at the ring electrode for glassy carbon.

It is noteworthy that in acetonitrile no soluble superoxide can be detected in 0.1 M lithium containing solutions with the rotating ring disk electrode;[9] however addition of only 0.1 M DMSO to 0.1 M $LiClO_4$ in acetonitrile yields soluble O_2^- which can be detected at the ring electrode due to the preferential solvation of Li^+ which stabilizes soluble O_2^- from disproportionation.[16]

The ring current maxima indicates that the surface concentration of soluble O_2^- increases the larger the ORR overpotential and then decreases due to either disproportionate or a two electron transfer to O_2 from the electrode, according to the accepted mechanism:.[9,13,26,27]

$$O_2 + Li^+ + e \rightarrow [O_2Li]_{surf} \quad [2]$$

$$[O_2Li]_{surf} + [O_2Li]_{surf} \rightarrow Li_2O_{2\downarrow} + O_2 \quad [3]$$

$$[O_2Li]_{surf} + Li^+ + e \rightarrow Li_2O_{2\downarrow} \quad [4]$$

Since the ORR product Li_2O_2, is insoluble[27] blocking the electron transfer at the electrode surface is observed in the reverse scan both on disk and ring electrodes. We have investigated the removal of oxygen reduced species from the electrode surface by exploring different potential windows as shown in Figure 3. When opening the potential window to 4.7 V for 10 seconds (panel A), the second potential scan shows complete recovery of both disk and Au ring currents. Panel B shows that starting the potential sweep at 3.8 V after a 10 second oxidation, subsequent lower cathodic currents are observed at disk and ring electrodes because of partly blockage by remaining oxygen reduction products on the surface. Finally, if we restrict the positive potential limit to 3 V for 10 seconds, the GC disk electrode surface is completely blocked with negligible disk and ring currents. These results are consistent with previous reports from Abraham[10] and the IBM group,[28] and also with recent surface morphology study by AFM on highly oriented pyrolytic graphite (HOPG),[25] Electrochemical quartz crystal microbalance (EQCM) on Au and X-Ray Photoelectron Spectroscopy (XPS)[29] experiments on HOPG and Au during oxygen reduction in $LiPF_6$ in DMSO.

The oxidation and removal of LiO_2 and Li_2O_2 and solvent and electrolyte decomposition products extends over a wide potential range[30] as can be seen from the anodic current in Figure 3A due to side reactions of Li_2O_2 with the solvent and electrolyte salt. Therefore, in order to obtain a reproducible fresh surface for each new experiment we have applied a high oxidation over potential where most ORR species at the surface are removed. A potential larger than 4.2 V is necessary to fully oxidize surface species formed during cycling. It should be mentioned that above 4.3 V oxidation of DMSO on Au has been observed by SNIFTIRS experiments in 0.1 M $LiPF_6$ in DMSO with detection of dimethyl sulfone.[14] We have thus adopted as a pretreatment of the GC and Au surfaces an oxidation potential of 4.2 V during 60 seconds and found then reproducible cyclic voltammetry curves for the ORR in DMSO/$LiPF_6$.

Since both potential and time are convoluted in the potential sweep experiments described, we have studied RRDE chronoamperometric transients for potential steps at the disk electrode from the positive potential limit (4.2 V) to different final electrode potentials in the ORR potential region. To our best knowledge these are the first experimental evidence of RRDE transient experiments of oxygen cathodes in lithium containing aprotic solvents.

Figures 4 and 5 depict typical disk and ring current transients for Au/Au and GC/Au electrodes RRDE electrodes at selected potentials in the ORR potential window. On both surfaces, the disk currents drop as the surface is progressively passivated by ORR insoluble products as confirmed by the mass uptake in EQCM experiments (see Figure 6 below). The ORR currents, I, can be corrected by the oxygen

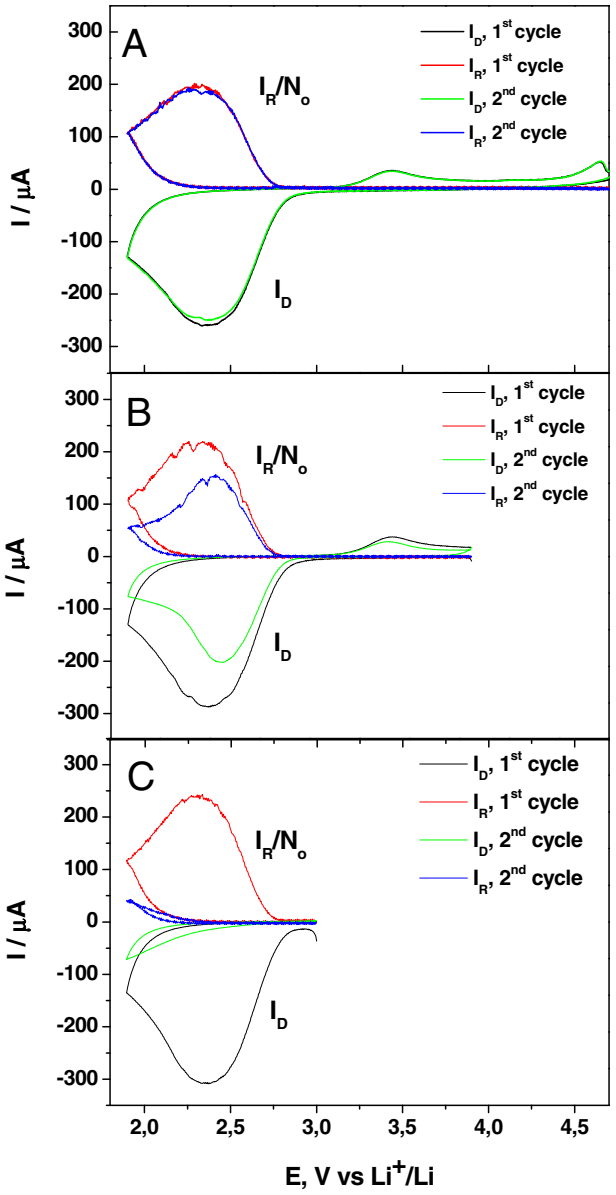

Figure 3. O_2 reduction polarization curves on a GC disk electrode in O_2 (1 atm) saturated 0.1 M $LiClO_4$ in anhydrous DMSO at W = 9 Hz (540 rpm) and scan rate of 0.1 V s^{-1} (lower curves) and O_2^- oxidation Au ring current normalized by the collection efficiency (I_R/No) at E_R = 3 V (upper curves) for different starting potentials: A) 4.7 V; B) 3.8 V and C) 3.0 V.

concentration depleted at the surface:

$$C^s_{o_2} = C^\infty_{o_2}\left(1 - \frac{I}{I_{Lim}}\right) I_{Lim} \quad [5]$$

where superscripts s and ∞ stand for surface and bulk O_2 concentrations respectively, and the I_{Lim} is the respective Levich convective-diffusion limiting current at 9 Hz (540 rpm) (c.a. 720 $\mu A.cm^{-2}$) for the two- electron O_2 reduction to Li_2O_2.

The soluble superoxide oxidation ring currents recorded simultaneously exhibit a peak at the different disk electrode potentials which reflect the outward flux of soluble LiO_2 from the disk into the electrolyte. The time evolution for these transients (c.a. > 1–10 s) is much longer than the transient time for the convective-diffusion flux from disk to ring, c.a. 300 ms at 9 Hz (540 rmp)[31,32] so that the transient reflects the flux on the disk surface. Notice that the ring currents are lower than the expected values from the geometric respective collection efficiency factors since most of the charge is accumulated on the

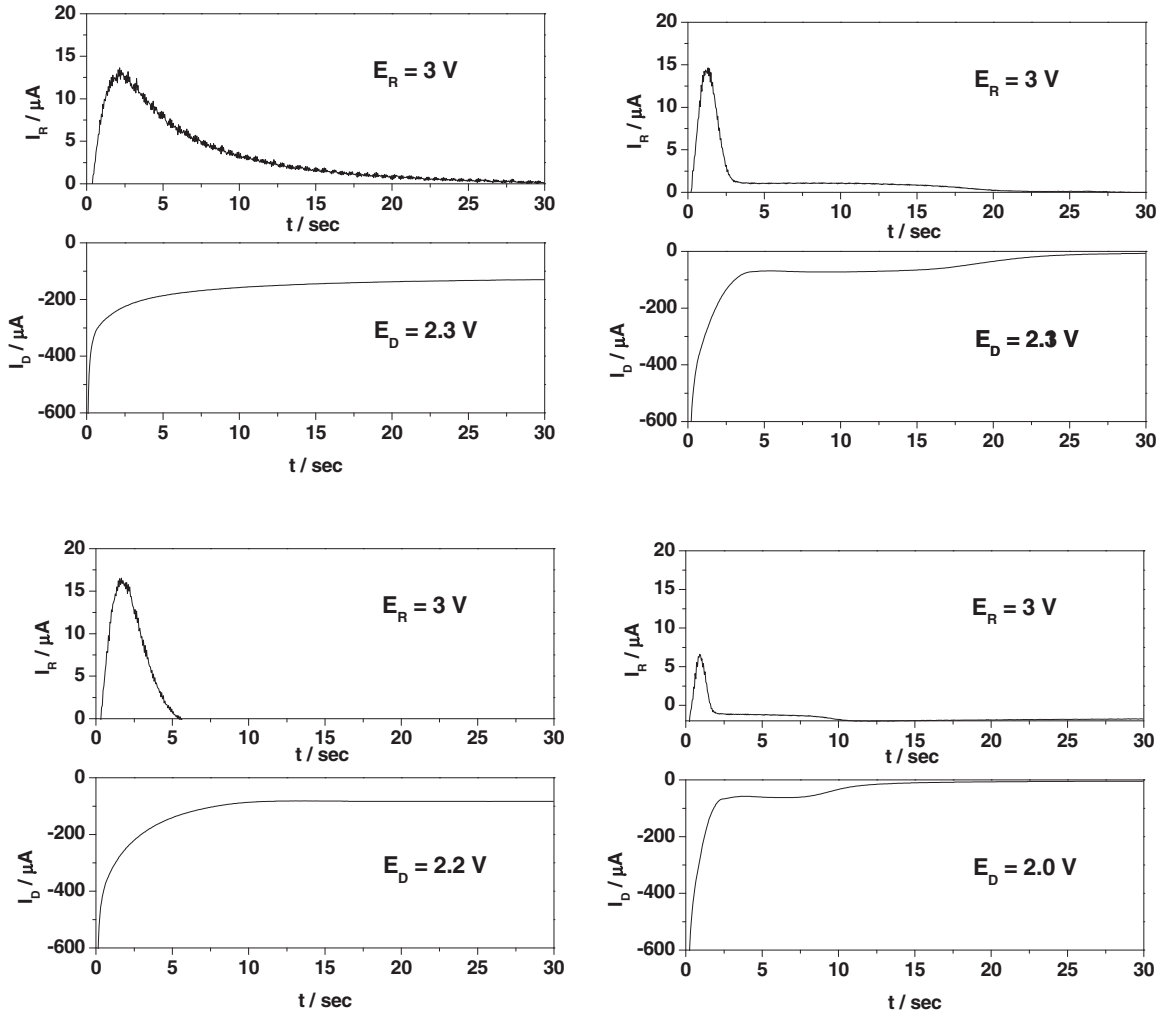

Figure 4. Chrono-amperometric transients for the reduction of O_2 on a RRDE Au disk electrode at 2.3, 2.2, 2.1 and 2.0 V in 0.1 M $LiPF_6$ in anhydrous DMSO at W = 9 Hz (540 rpm) (lower panel) and scan and O_2^- oxidation Au ring transient current at E_R = 3 V (upper panel). A_D = 0.2 cm^2, No = 0.28. Potential step at the disk electrode from 4.2 V to the values indicated in each panel.

disk electrode surface as Li_2O_2 and detected as a mass gain in EQCM experiments.

The disk current decay corresponds to the electrochemical reduction of O_2 on the Au partly covered by an insoluble Li_2O_2 deposit that progressively blocks electron transfer at the surface. The ORR constant disk current decreases the higher over potential and suggests that the oxygen reduction still can proceed on a Li_2O_2 thin film but at a lower rate until a critical peroxide film thickness is reached.

The electrochemical quartz crystal microbalance (EQCM) offers the unique possibility to measure the mass deposited in comparison with the charge passed, thus enabling the distinction between different molar masses deposited per Faraday of charge. Furthermore, neutral molecules like solvent can be detected if co-deposited on the surface. In a recent communication[33] we have suggested the co-deposition of solvent from EQCM evidence of mass per electron deposited much larger than any value expected from reactions.[2–4] This has been interpreted by the uptake of strongly bound DMSO to lithium ions when Li_2O_2 is deposited from oxygen reduction in DMSO based electrolyte.

EQCM experiments show that the Li_2O_2 is in the order of micrograms per square centimeter, much larger than expected coverage for a lithium peroxide monolayer,[34] c.a. 260 µC.cm^{-2} or 135 ng.cm^{-2}. Since lithium peroxide is an insulator, the flux of electrons from the underlying substrate across the Li_2O_2 film to the O_2 molecules adjacent to the surface would limit the ORR. As the poorly conducting film thickness increases charge transport through the growing Li_2O_2 film to the Li_2O_2-electrolyte interface is limited[35] and the O_2 current drops to zero at a critical thickness.

It is interesting to compare simultaneous disk and ring electrode current transients at potentials where O_2 reduction takes place. While the disk current decays monotonously, the ring current transient shows a maximum at short times. The ring currents are always a small fraction of the geometric collection efficiency so that the fraction of soluble superoxide is very small. Most of the superoxide formed by the reduction of oxygen results in the deposit of insoluble Li_2O_2 and only a small fraction can be collected at the ring electrode downstream. Furthermore, the ring peak current for the collection of superoxide ion under convective-diffusion conditions at constant disk potential exhibits a disk electrode potential dependence and goes through a maximum as shown in Figure 7. The maximum ring current at 2.2 V can be explained by the interplay between the buildup of surface O_2^- concentration at the disk electrode with further bimolecular disproportionate (eqn. 3) at low cathodic over potentials or direct two electron reduction at higher over potentials:

$$O_2 + 2Li^+ + 2e \rightarrow Li_2O_{2^-} \downarrow \qquad [6]$$

These processes are summarized in the following scheme, where Z = 1.4554 $D_{O2}{}^{1/2}\nu^{-1/6}C_{O2}$ and W is expressed in Hz (or Z = 0.62 $D_{O2}{}^{1/2}\nu^{-1/6}C_{O2}$ if ω is expressed in rpm).

While in Figures 1 and 2 the ring current shows a peak with potential, this is convoluted with time since the potential varies linearly

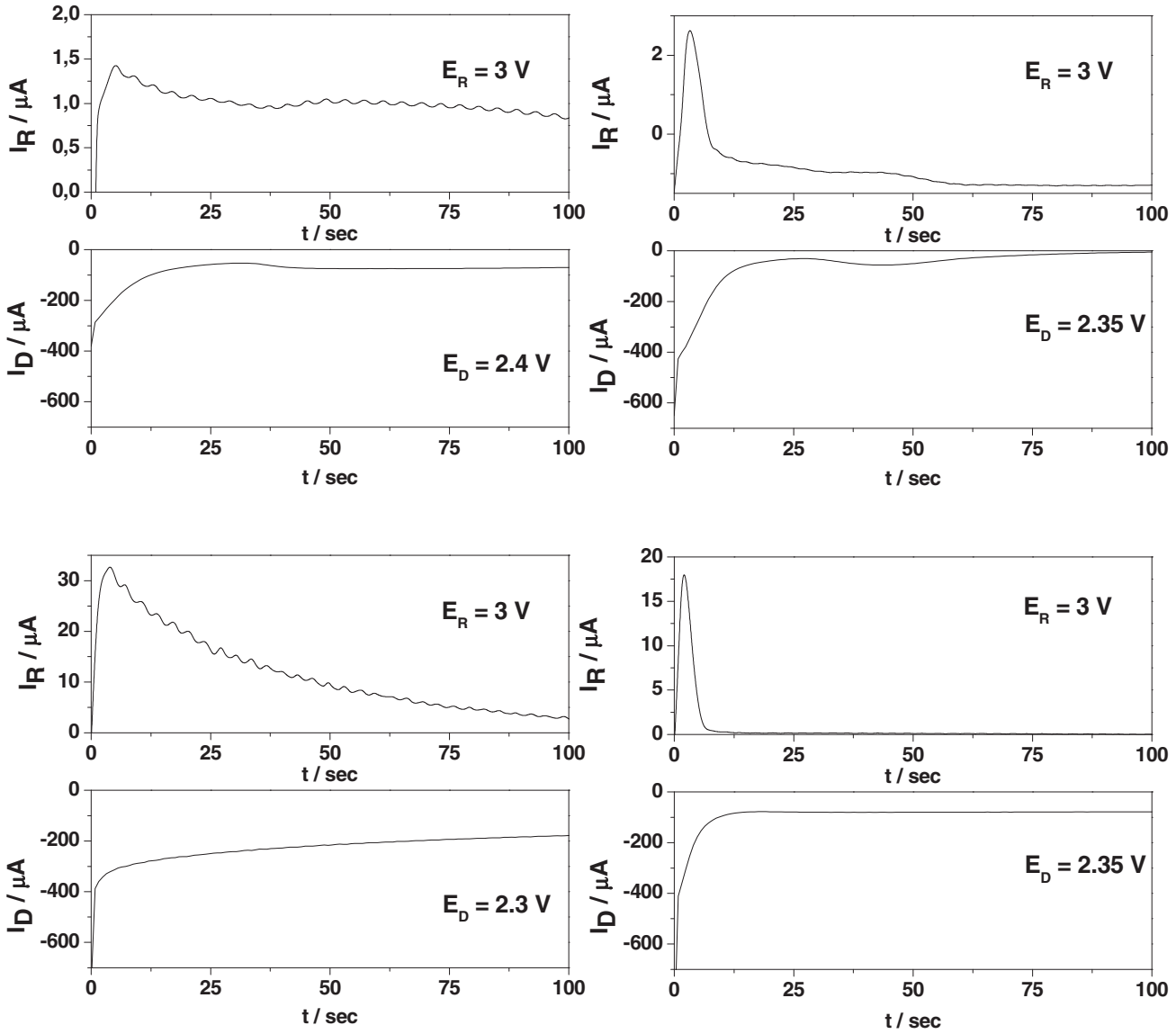

Figure 5. Chrono-amperometric transients for the reduction of O_2 on a RRDE GC disk electrode at 2.4, 2.35, 2.30 and 2.20 V in 0.1 M $LiPF_6$ in anhydrous DMSO at W = 9 Hz (540 rpm) (lower panel) and scan and O_2^- oxidation Au ring transient current at E_R = 3 V (upper panel). A_D = 0.2 cm^2, No = 0.32. Potential step at the disc electrode from 4.2 V to the values indicated in each panel.

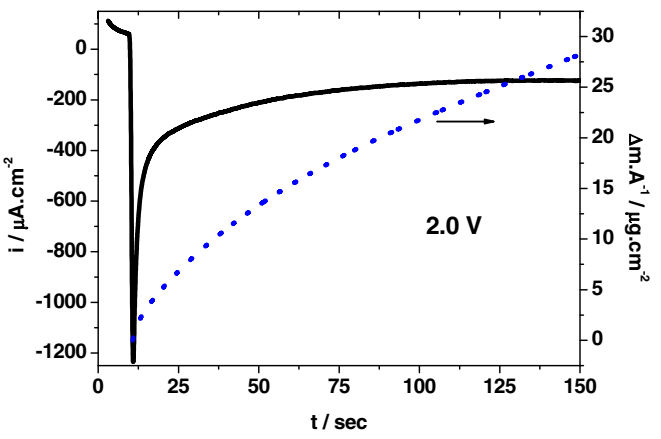

Figure 6. Chrono-amperometric transients for the reduction of O_2 on a Au coated quartz disk electrode at 2.0 V in 0.1 M $LiPF_6$ in anhydrous DMSO (solid line) and simultaeous EQCM mass gain (Δm/A).

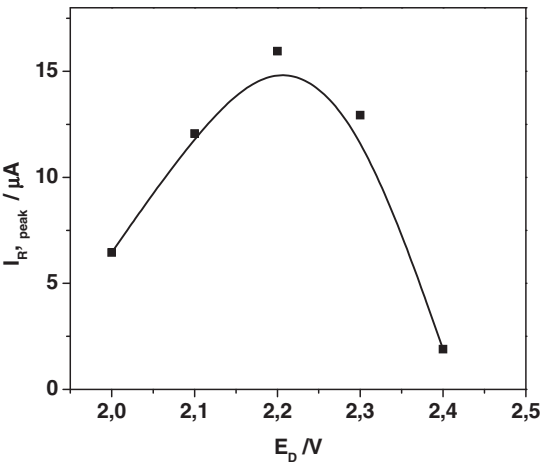

Figure 7. O_2^- oxidation Au ring current at the peak for different Au disk electrode potentials for data in Figure 4.

$$
\begin{array}{c}
Li_2O_{2\downarrow} + O_2 \\
\uparrow \\
O_2 + Li^+ + e \rightarrow [O_2^-]_{surf}[Li^+]_{surf} \quad + e + Li^+ \rightarrow Li_2O_{2\downarrow} \\
\downarrow \\
\left[O_2^-\right]_{DMSO}\left[Li^+\right]_{DMSO} \\
\downarrow ZW^{1/2}
\end{array}
$$

Scheme I. Scheme of reaction.

with time. It noteworthy in Figures 4 and 5 at 2.3 and 2.2 V the ring currents have dropped to zero there still is a disk current. Therefore at short times oxygen reduction results in soluble superoxide detected at the ring and insoluble lithium peroxide deposited at the disk as shown by the EQCM, but at longer times the collection of superoxide at the ring vanishes completely while the disk still records oxygen reduction cathodic current. Therefore there is a branching point as shown in the Scheme I. We, thus speculate that at longer times either dismutation or 2-electron O_2 reduction prevails over the one-electron reduction to peroxide. Another possible interpretation could be that the soluble superoxide is produced at the bare electrode while oxygen reduction still takes place on the covered Li_2O_2 patches. The ring current is always less than the value expected for the quantitative collection of superoxide formed on the ring, i.e. $I_R.N_o^{-1}$, while the EQCM detects solid deposit with a mass per electron larger than 39 g per Faraday expected for LiO_2 deposit or 23 g per Faraday expected for Li_2O_2 and this has been interpreted as co-deposition of solvent[33] which undergoes further decomposition by contact with lithium peroxide as seen from XPS evidence.[29]

Conclusions

We have studied the O_2 reduction reaction (ORR) on gold and glassy carbon electrodes in $LiPF_6$ electrolyte in DMSO solutions using the rotating ring disk electrode. With the Au ring soluble superoxide radical anion produced by one-electron reduction of O_2 has been detected by electrochemical oxidation at 3.0 V vs. Li/Li^+ in DMSO under convective-diffusion conditions. Only a small fraction of the O_2 flux at the disk electrode results in soluble superoxide collected at the ring.

For both glassy carbon and gold cathodes, typical oxygen reduction current-potential curves are sensitive to rotation speed and undergo a maximum with passivation by formation of a thick Li_2O_2 deposit while the Au ring electrode currents follow the same peak shape with detection of superoxide at the ring downstream the electrolyte solution.

Chrono-amperometric transients at the RRDE allowed to distinguish time and potential effects on the disk and ring currents. A small fraction of the stable LiO_2 thus diffuses out in solution and is detected at the ring electrode at short times. This ring current peak shows a maximum yield of soluble superoxide which depends on the disk electrode potential.

Both the preferential solvation of Li^+ in DMSO electrolyte with stabilization of soluble O_2^- and the disproportionation of adsorbed superoxide assisted by the conductive electrode surface are relevant to the lithium air battery technology.

Acknowledgment

Financial support from ANPCyT PICT grant No. 2037/2008 and FS-Nano 07 are greatly acknowledge. WT and AT acknowledge research scholarships from CONICET (Argentina).

Abbreviations

Cyclic Voltammetry, CV; Rotating Disk Electrode, RDE; Rotating Ring Disk Electrode, RRDE, Oxygen Reduction Reaction, ORR, Electrochemical Quartz Crystal Microbalance, EQCM.

References

1. P. G. Bruce, S. A. Freunberger, L. J. Hardwick, and J.-M. Tarascon, *Nature Materials*, **11**, 19 (2012).
2. J. Christensen, P. Albertus, R. S. Sanchez-Carrera, T. Lohmann, B. Kozinsky, R. Liedtke, J. Ahmed, and A. Kojic, *Journal of the Electrochemical Society*, **159**, R1 (2012).
3. L. J. Hardwick and P. G. Bruce, *Current Opinion in Solid State & Materials Science*, **16**, 178 (2012).
4. K. M. Abraham, in *Lithium Batteries: Advanced Technologies and Applications*, First ed., K. M. A. Bruno Scrosati, Walter van Schalkwijk, and Jusef Hassoun Editor, John Wiley & Sons, Inc (2013).
5. K. M. Abraham and Z. Jiang, *Journal of the Electrochemical Society*, **143**, 1 (1996).
6. T. Ogasawara, A. Debart, M. Holzapfel, P. Novak, and P. G. Bruce, *Journal of the American Chemical Society*, **128**, 1390 (2006).
7. C. O. Laoire, S. Mukerjee, K. M. Abraham, E. J. Plichta, and M. A. Hendrickson, *Journal of Physical Chemistry C*, **114**, 9178 (2010).
8. B. D. McCloskey, D. S. Bethune, R. M. Shelby, G. Girishkumar, and A. C. Luntz, *Journal of Physical Chemistry Letters*, **2**, 1161 (2011).
9. M. J. Trahan, S. Mukerjee, E. J. Plichta, M. A. Hendrickson, and K. M. Abraham, *Journal of the Electrochemical Society*, **160**, A259 (2013).
10. C. O. Laoire, S. Mukerjee, K. M. Abraham, E. J. Plichta, and M. A. Hendrickson, *Journal of Physical Chemistry C*, **113**, 20127 (2009).
11. K. Izutsu, *Electrochemistry in Non Aqueous Solutions*, Wiley-VCH, Weinheim, Germany (2002).
12. D. Xu, Z.-l. Wang, J.-j. Xu, L.-l. Zhang, and X.-b. Zhang, *Chemical Communications*, **48**, 6948 (2012).
13. Z. Peng, S. A. Freunberger, Y. Chen, and P. G. Bruce, *Science*, **337**, 563 (2012).
14. N. Mozhuzhukina, L. P. Mendez De Leo, and E. J. Calvo, *Journal of Physical Chemistry C.*, **117**, 18375 (2013).
15. Y. Chen, S. A. Freunberger, Z. Peng, O. Fontaine, and P. G. Bruce, *Nature Chemistry*, **5**, 489 (2013).
16. E. J. Calvo and N. Mozhzhukhina, *Electrochemistry Communications*, **31**, 56 (2013).
17. N. Mozhzhukhinaa, R. Semino, G. Zaldivar, D. H. Lariaa, and E. J. Calvo, *journal of Chemical Physicas*, submitted (2014).
18. D. Sharon, M. Afri, M. Noked, A. Garsuch, A. A. Frimer, and D. Aurbach, *Journal of Physical Chemistry Letters*, **4**, 3115 (2013).
19. D. G. Kwabi, T. P. Batcho, C. V. Amanchukwu, N. Ortiz-Vitoriano, P. Hammond, C. V. Thompson, and Y. Shao-Horn, *Journal of Physical Chemistry Letters*, **5**, 2850 (2014).
20. R. Younesi, M. Hahlin, and K. Edstrom, *Acs Applied Materials & Interfaces*, **5**, 1333 (2013).
21. C. J. Barile and A. A. Gewirth, *Journal of the Electrochemical Society*, **160**, A549 (2013).
22. B. D. McCloskey, A. Valery, A. C. Luntz, S. R. Gowda, G. M. Wallraff, J. M. Garcia, T. Mori, and L. E. Krupp, *Journal of Physical Chemistry Letters*, **4**, 2989 (2013).
23. J. W. Albery and M. Hitchman, *Rotating Ring Disc Electrodes*, Oxford University Press, Oxford (1971).
24. C. O. Laoire, S. Mukerjee, E. J. Plichta, M. A. Hendrickson, and K. M. Abraham, *Journal of the Electrochemical Society*, **158**, A302 (2011).
25. S. E. Herrera, A. Y. Tesio, R. Clarenc, and E. J. Calvo, *Physical Chemistry Chemical Physics*, **16**, 9925 (2014).
26. Z. Peng, S. A. Freunberger, L. J. Hardwick, Y. Chen, V. Giordani, F. Barde, P. Novak, D. Graham, J.-M. Tarascon, and P. G. Bruce, *Angewandte Chemie-International Edition*, **50**, 6351 (2011).
27. D. Sharon, V. Etacheri, A. Garsuch, M. Afri, A. A. Frimer, and D. Aurbach, *Journal of Physical Chemistry Letters*, **4**, 127 (2013).
28. B. D. McCloskey, A. Speidel, R. Scheffler, D. C. Miller, V. Viswanathan, J. S. Hummelshoj, J. K. Norskov, and A. C. Luntz, *Journal of Physical Chemistry Letters*, **3**, 997 (2012).
29. F. Marchini, W. Torres, S. Herrera, A. Tesio, E. J. Calvo, and W. F. J., in preparation (2014).
30. B. M. Gallant, D. G. Kwabi, R. R. Mitchell, J. Zhou, C. V. Thompson, and Y. Shao-Horn, *Energy & Environmental Science*, **6**, 2518 (2013).
31. A. J. Bard and L. R. Faulkner, *Electrochemical Methods. Fundamentals and Applications*, John Wiley & Sons, New York (2001).
32. J. Herranz, A. Garsuch, and H. A. Gasteiger, *Journal of Physical Chemistry C*, **116**, 19084 (2012).
33. W. R. Torres, A. Y. Tesio, and E. J. Calvo, *Electrchemistry Communications* (2014), in press.
34. S. Meini, M. Piana, N. Tsiouvaras, A. Garsuch, and H. A. Gasteiger, *Electrochemical and Solid-State Letters*, **15**, A45 (2012).
35. V. Viswanathan, K. S. Thygesen, J. S. Hummelshoj, J. K. Norskov, G. Girishkumar, B. D. McCloskey, and A. C. Luntz, *Journal of Chemical Physics*, **135** (2011).